# MICROWAVE MEASUREMENT OF eCLOUD USING RESONANT CAVITY TECHNIQUE IN THE MAIN INJECTOR

R. Cruz-Torres[a], J. C. T. Thangaraj[b], R. Thurman-Keup[b], and B. J. Fellenz[c]

[a]University of Florida, Gainesville, Florida 32605, USA
[b]Accelerator Physics Center, Fermi National Accelerator Laboratory, Illinois 60510, USA
[c]Accelerator Division, Fermi National Accelerator Laboratory, Illinois 60510, USA

*Abstract*

One of the main limitations of high-intensity proton beam accelerators is the formation of electron cloud (hereafter eCloud) inside the beam pipe. The presence of eClouds in the beam pipe has shown to cause some negative effects such as increase of vacuum pressure, emittance growth, and tune shift, therefore limiting the performance of the accelerator [1]. eClouds have been studied in the Main Injector (MI) at Fermilab using retarding field analyzers (RFAs) [2]. However, microwave phase shift has been tested as a technique that offers other advantages in the studying of eClouds in both experiments [3] and simulations [4]. Furthermore, a method was proposed and tested in the lab, consisting of the installation of reflectors to enhance the phase shift of the waves [5]. In this paper, we report the first measurements using this technique in a small section of the MI-20 beam pipe.

## INTRODUCTION

By sending electromagnetic microwaves through an electron cloud of uniform distribution and measuring the phase shift of these waves, the electron cloud density (ECD) can be measured [3]. For a cold, homogeneous electron distribution that completely fills the beam channel and with no external magnetic field, the wave dispersion relationship for a TE mode is given by [4]:

$$k^2 = \frac{\omega^2 - \omega_c^2 - \omega_p^2}{c^2} \tag{1}$$

Where $k$ is the wave number, $\omega_p$, $\omega$, and $\omega_c$ are respectively the frequency of the cold plasma , the input frequency, and the cut-off frequency of the waveguide. Also, in this equation $c$ is the speed of light. $\omega_p$ is related to the ECD $\rho$ through [1]:

$$\omega_p^2 = 4\pi\rho r_e c^2 \tag{2}$$

Where $c$ is the speed of light and $r_e$ is the classical electron radius. If the wave propagates a distance $L$, then the phase advance it experiences is given by $kL$ [4], and therefore if we compute the difference between the phase advance with and without eCloud respectively, we get [4]:

$$\varphi = [\sqrt{\omega^2 - \omega_c^2} - \sqrt{\omega^2 - \omega_c^2 - \omega_p^2}]\frac{L}{c} \tag{3}$$

If we perform a Taylor expansion of the second square root in equation (3) for small values of $\omega_p$ up to the quadratic term term we obtain:

$$\sqrt{\omega^2 - \omega_c^2 - \omega_p^2} \approx \sqrt{\omega^2 - \omega_c^2} - \frac{\omega_p^2}{2\sqrt{\omega^2 - \omega_c^2}} \tag{4}$$

Substituting equation (4) into equation (3) we get that the phase shift of an electromagnetic wave of frequency $\omega$ through an uniform, cold plasma per unit length is given by [1]:

$$\varphi/L \approx \frac{\omega_p^2}{2c\sqrt{\omega^2 - \omega_c^2}} \tag{5}$$

This technique was first proposed in Berkeley [3]. At Fermilab, different ECD studies have been carried out with and without absorbers using this technique. Absorbers are installed as a way to avoid microwave signal coming from other parts of the machine. The limitation with this technique is that the measured signal is small due to the absorptions. We, on the other hand, decided to install reflectors. After some years of testing this technique in bench-top experiments [1] [6], it was implemented in the MI ring.

## EXPERIMENTAL SETUP

The experiment was carried out in a 13-meter-long section of the MI elliptical pipe. The dimensions of the major and minor radii of this ellipse are 59.82 mm and 26.55 mm respectively. The thickness of the pipe is 1.65 mm. Two detectors were installed at both ends of this section. In between, there are two Fermilab Main Injector (FMI) 240" dipoles. The connection between the beam pipe and the equipment located in the service building was made using low loss 1/4" Superflex Heliax cables allowing for a loss of 5 dBm per cable only. Each detector consist of a small section of the elliptical pipe that contains two horizontally oriented antennas and one ear behind each antenna, as shown in Fig.1 and Fig.2. The gap between the ear and the antenna is different on both sides of each detector, allowing for different configurations to be tested. The ears are made of 316l stainless steel and serve three main functions. First, they act as the previously mentioned reflectors for low frequencies. Second, they close the pipe in the sense that create a cavity-like space, thus increasing the phase shift. Finally, they protect the antennas from beam loss.

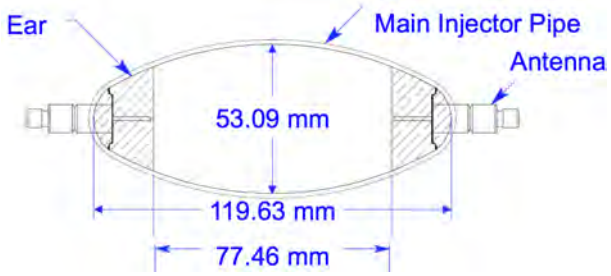


Figure 1: Mechanical drawing showing cross section of the detector. The shaded area represents the reflecting ears.

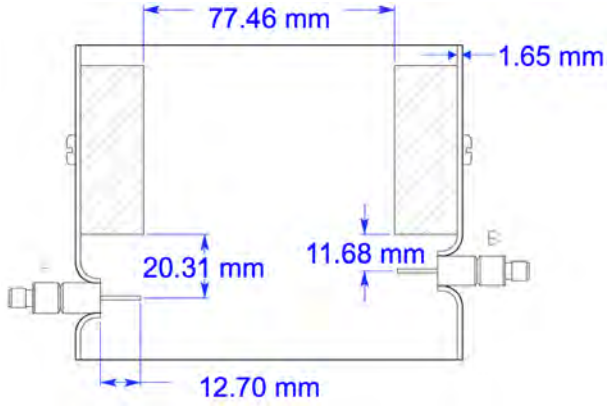


Figure 2: Mechanical drawing showing top view of the detector. The shaded area represents the reflecting ears. The difference in distance between each antenna and the corresponding ear can be seen in the picture.

A TE microwave with a frequency slightly above the cut-off frequency of the beam pipe is generated using an Agilent E4428C signal generator of bandwidth 250 kHz to 6.0 GHz. Equation (5) suggests that it is better for the input frequency to be as close to the cut-off frequency as possible to enhance the phase shift. This electromagnetic wave is then amplified making use of an Avantek APG4004N311 power amplifier. This amplifier is shown in Fig.3 as (5). The amplified signal travels from the input antenna through the eCloud existing inside the pipe. At this point the microwave suffers a phase shift before arriving at the output antenna. The phase-shifted signal is then studied by the means of an Agilent N9020A spectrum analyzer of bandwidth of 20 Hz to 13.6 GHz that allows for the measurement of the phase shift. The fraction of the microwave that travels away from the cavity is then reflected by the ears and bounces back and forth, allowing for the measurement of a large but at the same time localized signal. All the equipment was installed in a rack at the MI service building MI-20, as shown in Fig.3. We labeled the ports or antennas as shown in Fig.4. Ports 1 and 2 correspond to the two antennas located in the upstream detector; correspondingly, ports 3 and 4 are located in the downstream detector. Even numbers are on the inner side of the beam pipe and the distance between these antennas and the ear is 20.31 mm. Accordingly, odd numbers are on the outer side of the beam pipe and the distance between these antennas and the ear is 11.68 mm.

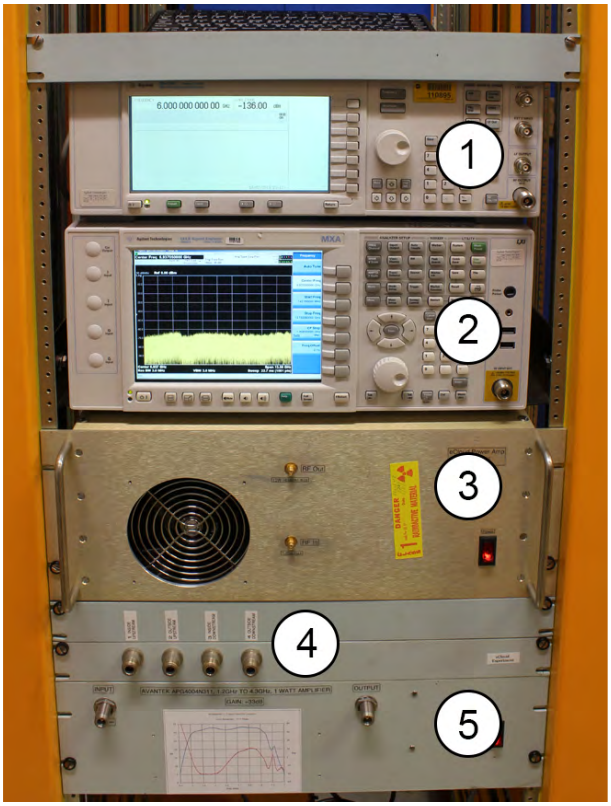


Figure 3: (1) Agilent signal generator; (2) Agilent spectrum analyzer; (3) Power amplifier I; (4) Antenna connectors; (5) Power amplifier II.

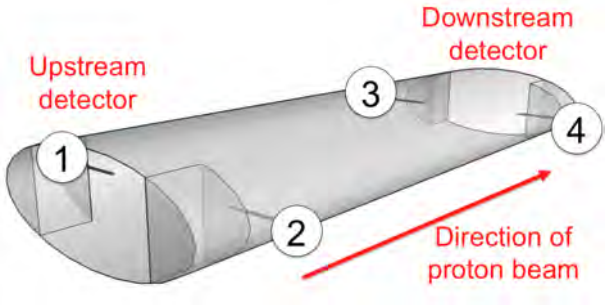


Figure 4: Labeling of the detectors. Ports 1 and 2 correspond to the two antennas located in the upstream detector; correspondingly, ports 3 and 4 are located in the downstream detector. Even (odd) numbers are on the inner (outer) side of the beam pipe.

## CALIBRATION OF THE EQUIPMENT

### *Amplifier bandwidth measurements*

We used two power amplifiers to carry out this experiment. For now on, we will call these amplifiers PA-I (listed as (3), as shown in Fig.3) and PA-II (listed as (5), as shown in Fig.3). PA-I is a 40-db-gain power amplifier. The calibration of this equipment reveals a maximum amplification in the range from 2 MHz to 2 GHz. The response curve is shown in Fig.5. For reasons that are explained in the next section, we had to switch to PA-II. This equipment is a 33-dB-gain Avantek APG4004N311 power amplifier of bandwidth of 1.2 GHz to 4.3 GHz that accepts up to 1 Watt of power. Its response curve is shown in Fig.6.

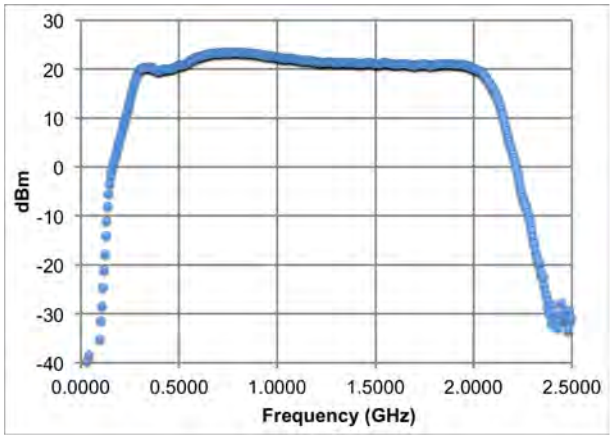


Figure 5: Response curve of power amplifier I (PA-I). This power amplifier has a 40-db-gain. This plot was made taking an S21 measurement and shows a maximum amplification in the range from 2 MHz to 2 GHz.

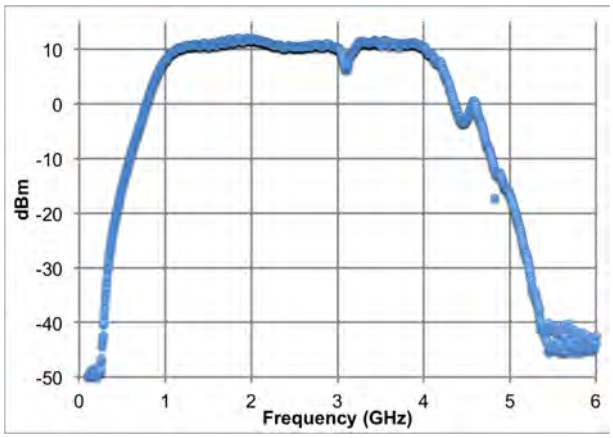


Figure 6: Response curve of power amplifier II (PA-II). This Avantek APG4004N31power amplifier has a 33-dB-gain. This plot was made taking an S21 measurement and shows a maximum amplification in the range from 1.2 GHz to 4.3 GHz.

### *S parameters and cut-off frequency*

The cut-off frequency is a threshold value below which the transmitted power for either a waveguide or a cavity is very small compared to the incident power. Therefore, it is necessary to work in a range of frequencies above the cut-off value in order to transmit a measurable signal. The cut-off frequency depends mainly on the transverse dimensions of the waveguide and the orientation of the antennas. The previously measured value for the elliptical pipe of MI was 1.52 GHz [7]. Therefore, we started the measurements using the power amplifier PA-I, which bandwidth occupies this range. However, after repeatedly taking S21 measurements without PA-I, we found a cut-off value of 3.6 GHz, as shown in Fig.7. Since PA-I's bandwidth is out of this range, we had to start using PA-II to take the measurements.

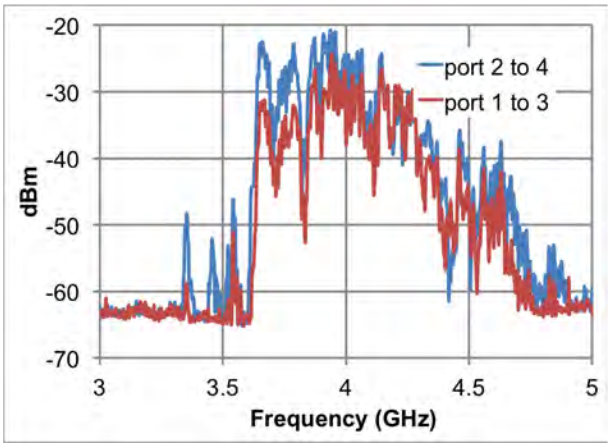


Figure 7: S21 measurement between antennas 1 and 3 (red) and antennas 2 and 4 (blue) showing both plots a cut-off frequency around 3.6 GHz. The measurement between antennas 2 and 4 (blue) exhibits a slightly higher amplitude than the measurement between antennas 1 and 3 (red). Therefore, this mode seems to be more efficient for the ECD measurement.

### *Cable dispersion*

In order to determine the cable dispersion, we connected an Agilent Fieldfox network analyzer directly into the detectors, as shown in Fig.8 in the tunnel and took S21 measurements. Then, measurements of the same type were taken from the service building MI-20 and compared with the ones from the tunnel. Following this method, a cable dispersion of approximately 5 dB was measured, as shown in Fig.9. As mentioned before, low loss 1/4" Superflex Heliax cables were employed to connect the detectors in the tunnel into the equipment at MI-20, allowing for a negligible cable loss.

## SIMULATIONS

In order to further study the discrepancy between the previously reported cut-off frequency (1.5 GHz) and the newly

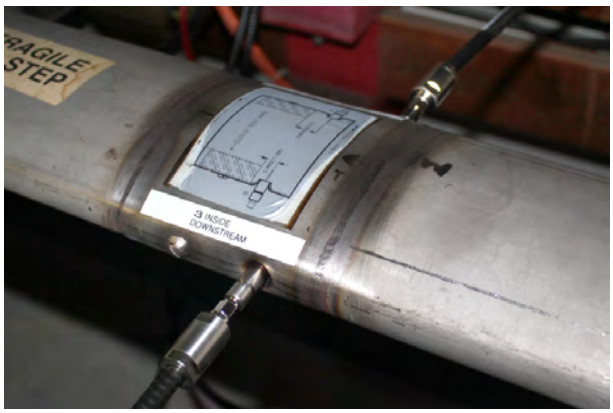

Figure 8: Photo of the downstream detector installed in the MI beam pipe. In this image, the proton beam travels from right to left. This picture shows the low loss 1/4" Superflex Heliax cables directly connected to the detectors.

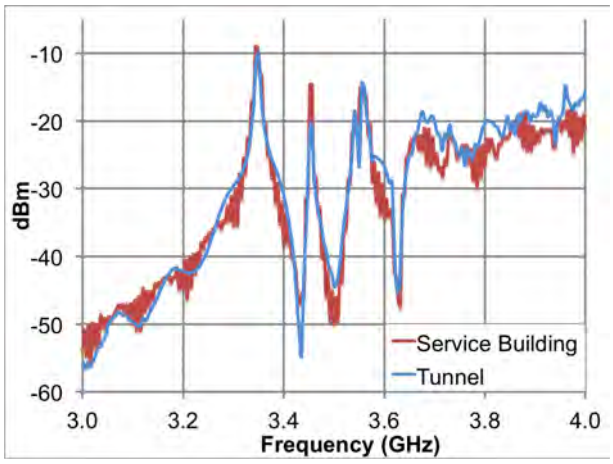


Figure 9: Cable dispersion. The use of low loss 1/4" Superflex Heliax cables to connect the equipment to the detectors in the beam pipe allows for a loss of 5 dBm per cable only. This can be verified measuring the amplitude difference between the S21 measurement taken connecting an Agilent Fieldfox network analyzer directly into the detectors in the tunnel (blue) and S21 measurements taken from the service building MI-20 (red).

measured one (3.6 GHz), four simulations were carried out using CST Microwave Studio. The simulation solves Maxwell's equations in the frequency domain for a given physical configuration and given excitation sources. In our case the physical configuration is the beam pipe, ears, and coaxial antennas. The excitation source is input on one of the coaxial ports and measurements are made at the other ports. The solving is performed on a tetrahedral mesh, and so far, the metal beam pipes and such have all been assumed to be perfect conductors. This assumption can be turned off to check for the effects of finite conductivity, however that will also slow down the simulation. The ends of the beam pipe are modeled as perfect matching layers, which means, that they have no effect on the fields. The inner dimensions of the pipe are 180 cm long, major radius of 6.15 cm, and minor radius of 2.65 cm. The distance between the closest antennas is 100 cm. The opposite antennas are separated by 101.726 cm. The ears are 50 mm long and are separated from the other pair by 104.062 cm.

### *Bench-top experiment simulation*

Following previously studied bench-top experiments using the same type of elliptical pipe [1] [6], we simulated dipole antennas, as shown in Fig.10. As shown in Fig.11, the cut-off frequency for this antenna mode from the simulation agrees with the value of 1.5 GHz, as previously measured in the lab.

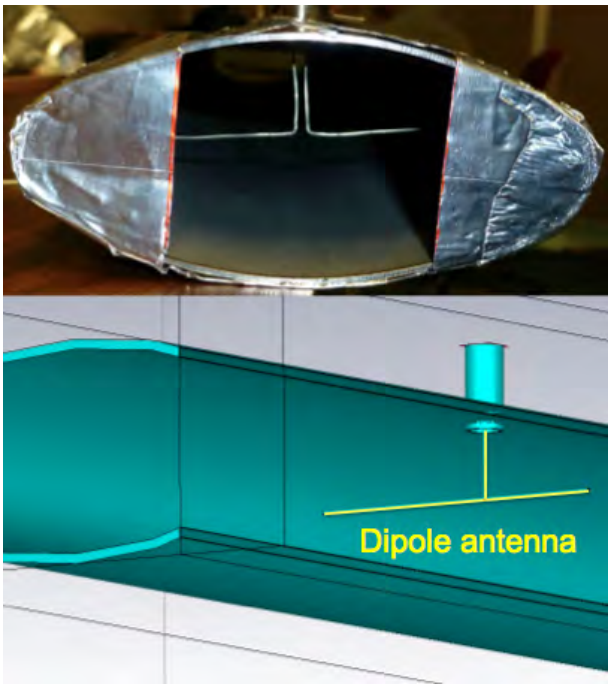


Figure 10: Bench-top experiment. Top: Photo of the cross section of the beam pipe used in a bench top experiment that studied the effects of reflecting ears in ECD measurements [1]. Bottom: Simulated setup using CST Microwave Studio, recreating the setup used in the bench-top experiment.

### *MI setup simulation*

The actual MI configuration of the detectors was simulated, as seen in Fig.12. This consists of horizontally oriented antennas and 21 mm ears to close the cavity. The gap between the ears is 77.46 mm. Using this configuration, a cut-off frequency above 3.0 GHz is measured from the simulation, as shown in Fig.13. Therefore, the simulation also agrees with the measurements taken using the actual detectors. The theories to explain these discrepancies at this point were either antenna configuration or length of the ears

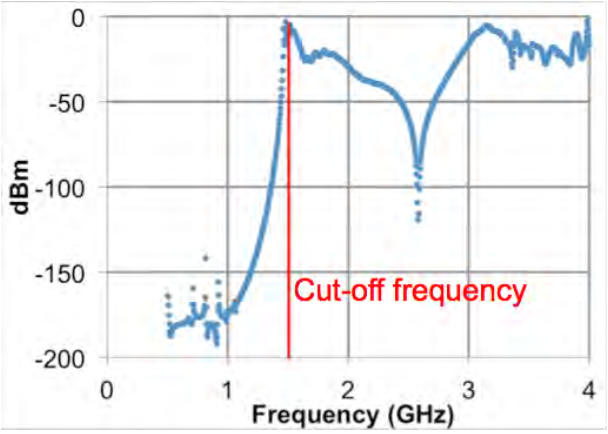


Figure 11: Data from simulation showing a cut-off frequency of 1.5 GHz for a dipole antenna mode corresponding to the bench-top experiments.

in the z direction. Ears geometry in the x-y plane was discarded because several measurements had been taken for different ear widths in the bench-top experiments, all of them yielding a cut-off frequency of 1.5 GHz.

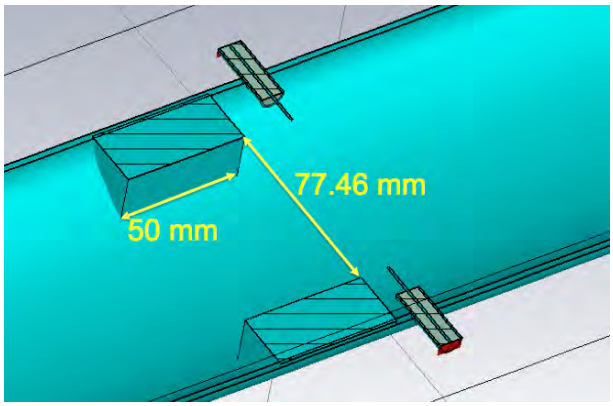


Figure 12: Simulation of the present setup of the eCloud detectors in the MI beam pipe to further study the discrepancy between the bench-top experiment and the direct measurement of the cut-off frequency in the accelerator beam pipe.

### *MI setup without ears simulation*

Also, when the ears were removed from the simulation, as shown in Fig.14, a cut-off frequency above 3.0 GHz is also measured. This shows that the difference between the cut-off frequency measured from the bench-top experiments and that measured in the MI beam pipe is due only to the antenna orientation and not to the ear configuration. Furthermore, these 21 mm wide ears do not seem to act like cavity walls at such high frequencies. Therefore, we decided to simulate wider ears.

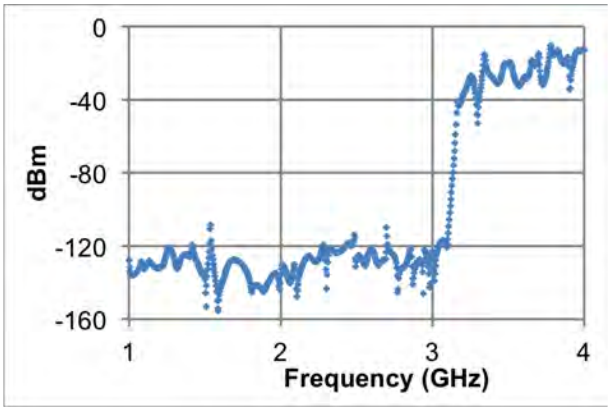


Figure 13: S21 from simulation of the present setup of the eCloud detectors, showing a cut-off frequency slightly above 3.0 GHz, agreeing with the cut-off frequency measured in the beam pipe of MI. Furthermore, no effect of the ears is seen.

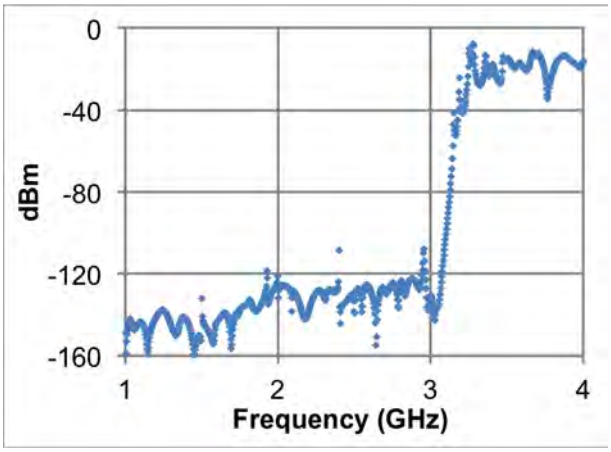


Figure 14: S21 measurement from simulation of the present setup of the eCloud detectors in the MI beam pipe without the ears. The same value of the cut-off frequency around 3.0 GHz is found. This indicates that the cut-off frequency is not being determined by the ears, but by the antennas. Furthermore, no effect of the ears is seen.

### *MI setup with wider ears*

We also simulated the case of wider ears, as shown in Fig.15. The space between the two ears is barely 18 mm, and therefore almost the entire pipe is closed. Still, we obtained the same cut-off frequency, as shown in Fig.16. This means that almost with an actual cavity, which is the whole beam pipe closed, the microwaves are exiting the cavity-like space rather than being reflected by the ears. The problem with constructing this type of ears is that it can disrupt the proton beam.

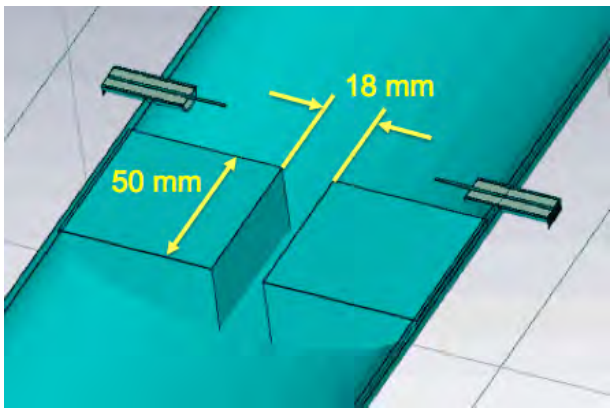


Figure 15: Simulation of the present setup of the eCloud detectors in the MI beam pipe with wider ears. In this setup, we set a gap of 18 mm between the ears. The problem with constructing this type of ears is that it can disrupt the proton beam.

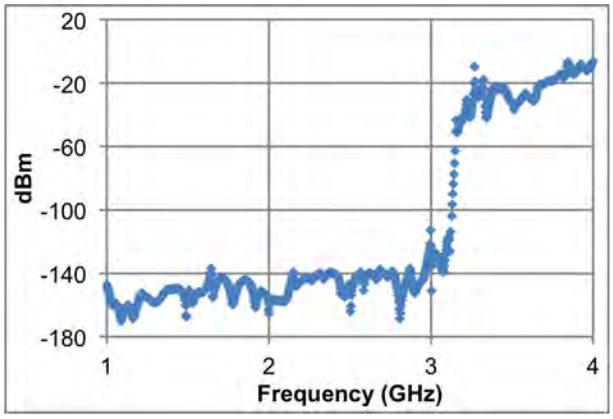


Figure 16: S21 from simulation of the present setup of the eCloud detectors in the MI beam pipe with wider ears. In this setup, we set a gap of 18 mm between the ears. For the horizontal antennas, even with these wide ears a cut-off frequency above 3.0 GHz is found. Furthermore, no effect of the ears is seen.

## ECD MEASUREMENT

We took the first ECD measurements with the MI in a testing stage, running at low energy and low intensity. At this point, the total number of bunches injected from the booster into the machine was 84, but due to the gap in the kicker, only 80 bunches were making their way into the MI beam pipe. The number of protons per bunch was $1.25 \times 10^8$, and therefore, the total number of protons in the beam pipe was $1 \times 10^{10}$. The energy of the protons was set to 120 GeV. The ECD depends mainly on the intensity of the proton beam. For such low parameters we predicted no measurable presence of eCloud. Effectively, when the measurement was taken, no presence of eCloud was found. This was checked up on measurements of the ECD taken from four RFAs that are installed in the MI beam pipe [8]. Further measurements are expected to be taken once the MI is cranked up to higher intensities in the near future.

## MAGNETIC LOOP AND FUTURE PLANS

In an attempt to find a solution to the difficulties experienced with the horizontally oriented antennas installed in the MI beam pipe, and taking into consideration that a setup with the antennas used in the bench-top experiment is not achievable since it disrupts the proton beam, a fifth simulation was carried out. It consisted of a magnetic loop antenna, as shown in Fig.17. This antenna couples a magnetic rather than an electric field. The vertical sections couple a signal similar to the one measured in the bench top experiment, shifting the cut-off frequency from above 3.0 GHz to about 1.5 GHz, as shown in Fig.18.

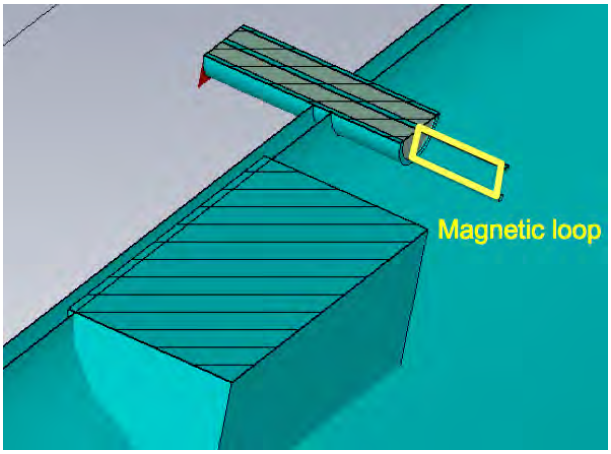


Figure 17: Simulation of magnetic loop antennas. This antenna mode is proposed to be installed in the MI beam pipe as a way to solve the cut-off frequency issue found in the current detector setup.

Furthermore, right after the cut-off frequency multiple peaks start to appear. These peaks are nodes that are caused by microwaves being reflected on the surface of the ears multiple times. The frequency of each one of these harmonic peaks can be found using the equation [1]:

$$f^2 = \frac{c^2}{4L^2} \times n^2 + f_c^2 \qquad (6)$$

In this equation, $f$ is the frequency of the node, $c$ is the speed of light, $L$ is the length of the cavity, $n$ is the harmonic number, and $f_c$ is the cutoff frequency. If we plot the different values of $f^2$ corresponding to the nodes vs. $n^2$, we get a linear function of slope $\frac{c^2}{4L^2}$ and intercept $f_c^2$, as shown in Fig.19.

The values obtained from the plot shown in Fig.19 for $L$ and $f_c$ correspond to the same values of the length of the pipe simulated and the previously measured cut-off frequency. This means that the installation of this magnetic loop antenna would facilitate the ECD measurements for

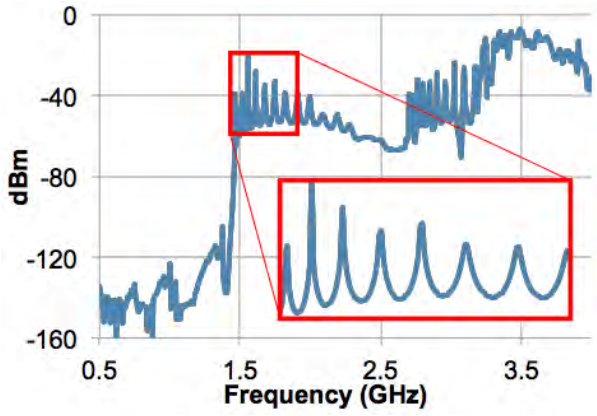


Figure 18: S21 from simulation of magnetic loop antennas. It is seen from the graph that for this setup, a cut-off frequency of 1.5 GHz is found. Furthermore, right after the cut-off frequency, certain nodes corresponding to microwave reflections begin to appear as shown in the red box, thus facilitating the ECD measurement.

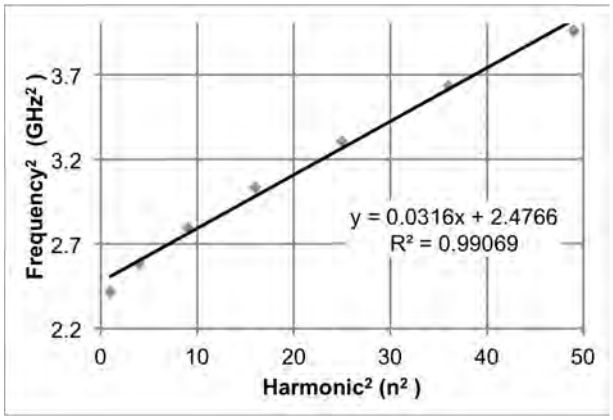


Figure 19: Linear plot of $f^2$ vs. $n^2$ showing that the peaks found in Fig.18 correspond to the standing waves obtained from equation (6). The slope of this linear fit corresponds to the value $\frac{c^2}{4L^2}$ and intercept corresponds to the value $f_c^2 = 2.4766$. Here, $f$ is the frequency of the node, $c$ is the speed of light, $L$ is the length of the cavity, $n$ is the harmonic number, and $f_c$ is the cutoff frequency.

both, the shift of the cut-off frequency back to 1.5 GHz and the presence of the nodes in this range caused by multiple reflections of the microwaves on the ears.

## CONCLUSIONS

- The theories explaining the shift of the cut-off frequency from the expected 1.5 GHz to the measured 3.6 GHz consisted of either the effect of the dimensions of the ears in the z direction or the orientation of the antennas. The former was discarded and the latter was indicated as highly probable thanks to the CST Microwave Studio simulations. As it turns out, the vertical orientation of the antennas better couples the electric field inside the beam pipe.
- The previous bench-top experiments [1] [6] helped discard the possibility of the width of the ears as being the cause of the cut-off frequency shift. Different ear widths were tested on these bench-top experiments. For all the widths tested, including the beam pipe totally closed, a 1.5 GHz cut-off frequency was measured.
- It is important to find a way to take the cut-off frequency back to 1.5 GHz, because for frequencies as high as 3.6 GHz the reflection effect of the ears seems to be negligible.
- A way of getting a cut-off frequency of 1.5 GHz again without disrupting the proton beam is by the installation of magnetic loop antennas as the ones shown before, or T-shaped antennas that can couple the vertical modes of the electric field inside the beam pipe.
- Before modifying any of the setup, it is important to retake the ECD measurements once the MI reaches a higher intensity. This measurement should also be compared to the ones measured using RFAs.

## ACKNOWLEDGEMENTS

I would like to thank a huge group of people that made this project possible. First of all, thanks to Heather Ray, Eric Prebys, Eric Ramberg, Linda Spentzouris and Carol Angarola, who fought and struggled, yet never gave up in the crusade of giving me an opportunity to come to Fermilab. Thanks to my mentor Jayakar Charles Thangaraj who is a great physicist and guide. Thanks again to him for his time and his effort, for pushing me forward, for supporting my project, for helping me make hard decisions, for being tough, and for being a friend. Thanks to the Lee Teng students from previous years who started my project and gave me the right path to follow. Thanks to my roommates Jack Bluebaugh, Bruce Howard, and Ariel Ruiz for all the support. Thanks in general to all my fellow interns, specifically to the Lee Teng students. Thanks to USPAS for all the effort and knowledge that was passed on to me. Thanks to Brian Fellenz who was able to gather everything we needed, and who never said no when I went requesting assistance. Thanks to Dr. Thurman-Keup, whose help with the CST simulations was vital. Thanks to Dr. Zwaska for always contributing with excellent ideas for the project. Thanks to the main control room operators for all the updates on the accelerator status and for facilitating the access to MI-20. Thanks to Dave Capista for all the information about the section of the beam pipe we used and the detectors. Thanks to Nathan Eddy for helping us gather the necessary equipment we used. Thanks to Jeffrey Eldred for supporting us and for helping us take some of the measurements. Thanks to Elvin Harms for repeatedly lending an Agilent Fieldfox network analyzer. Thanks to Denton Morris for playing a vital role in this project, for supporting the team, for answering many questions, and for being

always willing to take some time to help us. Last but not least, thanks to the Department Of Energy for opening the doors for me, for making valuable resources available to my cause, and for letting me have this incredible experience at Fermilab.

## REFERENCES

[1] H. Wang et al. "Microwave reflection technique for electron cloud density measurement". *Lee Teng Summer Internship, Fermilab*, 2011.

[2] M. Backfish. "Electron Cloud in Steel Beam Pipe vs Titanium Nitride Coated and Amorphous Carbon Coated Beam Pipes in Fermilab's Main Injector". *Masters Thesis, Fermilab*, 2013.

[3] S. Desantis et al. "Measurement of Electron Clouds in Large Accelerators by Microwave Dispersion". *Physical Review Letters*, 100, 2008.

[4] K. Sonnad et al. "Simulation and Analysis of Microwave transmission through an electron cloud a comparison of results". *Proceedings of PAC'07*, 2007.

[5] C. Tan. "Measuring electron cloud density with trapped modes". Fermilab (Unpublished).

[6] P. A. Kyaw et al. "Improving boundary conditions for microwave reflection to measure electron cloud density". *Lee Teng Summer Internship, Fermilab*, 2012.

[7] Y.-M. Shin et al. "Electron cloud density analysis using microwave cavity resonance". *IOP Publishing*, 2013.

[8] M. Backfish. "Measurement of ECD using RFAs". private communication, 2013.